第 50 卷 第 19 期/2023 年 10 月/中国激光 研究论文

中国激光

脉冲光的光纤布里渊散射谱拟合研究

杨志[1,2]，王震[1*]，李永倩[1,2]，吕安强[1,2]

[1]华北电力大学电子与通信工程系，河北 保定 071003；

[2]华北电力大学河北省电力物联网技术重点实验室，河北 保定 071003

摘要 针对脉冲光布里渊散射谱在用传统的洛伦兹曲线拟合时存在较大拟合误差的问题，通过理论分析推导出了脉冲光的光纤布里渊散射谱函数表达式。采用布里渊光时域反射(BOTDR)系统对一段3000 m长光纤的布里渊散射谱进行测量，对测得的不同脉冲宽度下的光纤布里渊散射谱分别采用洛伦兹函数和本文推导的函数进行拟合。结果表明：随着入射脉冲光的脉冲宽度变窄，采用推导的光纤布里渊散射谱函数能够有效提高BOTDR系统布里渊散射谱的拟合精度。

关键词 光纤光学；布里渊散射；布里渊频移；洛伦兹函数；数据拟合

中图分类号 TN247 **文献标志码** A **DOI**：10.3788/CJL221196

1 引 言

自1970年以来，光纤通信发展迅速，光纤传感因此也发展迅速并实现了大面积应用。光纤传感技术以其抗电磁干扰能力强、灵敏度高、测量频带宽、动态响应范围大等优点被广泛应用于航天航空[1]、电力检测[2]、医疗[3]、矿业[4]等领域。光纤分布式传感能够检测温度、应力等物理量沿光纤的分布。其中，基于布里渊散射效应的光纤分布式传感以其高精度、高灵敏度的特点受到了越来越多研究人员的青睐[5]。布里渊光时域反射(BOTDR)法是一种基于布里渊中心频率偏移与外界温度或应变变化的线性关系实现传感的技术，同时也是分布式传感工作中最常用的一种方法，可用于对许多大型工程进行安全检验[6-7]。

脉冲光(脉冲宽度大于声子寿命)注入光纤后会产生一个布里渊散射光。当传感光纤的温度或所受压力发生变化时，自发布里渊散射光谱的中心频率就会出现偏移。为了获得目标传感变量，需要提取出布里渊散射谱的中心频率。随着科技和工业的快速发展，现代工业传感应用要求的检测精度越来越高，时间延迟越来越小，因此，如何准确地提取出布里渊散射光谱的中心频率是实现外界环境检测的关键问题[8-11]。布里渊频移通常是通过拟合得到的。目前，通常利用洛伦兹函数进行布里渊散射光谱中心频率的提取。该方法比较简单，而且容易实现，因此被广泛使用[12-14]。单频连续光的布里渊散射谱满足洛伦兹函数分布。当进行脉冲调制时，入射信号的频谱被展宽，所得散射光的光谱同样被展宽，因此，通过一般的洛伦兹参数模型进行拟合无法得到更精确的模型拟合结果。经过理论研究，笔者推导出了脉冲光信号的光纤布里渊散射谱的函数表达式，有效提高了布里渊散射光谱的拟合准确度。

2 基本原理

2.1 常用布里渊散射拟合模型

自发布里渊散射是由在光纤中传播的光波和声波相互作用引起的非弹性光散射现象[15-16]。当连续单频光在光纤中传播时，由自发产生的声波在光纤中振荡的幅度随着时间延长呈指数型衰减[幅度-时间表达式为$\exp\left(-t/\Gamma_{\mathrm{B}}\right)$，其中$\Gamma_{\mathrm{B}}$是光纤中的声子寿命]，被声波散射的光波的振幅也呈指数型衰减。因此，自发布里渊散射的功率谱密度为洛伦兹函数，即

$$g_{\mathrm{B}(v)}=g_0\frac{\left(\Delta v_{\mathrm{B}}/2\right)}{\left(v-v_0\pm v_{\mathrm{B}}\right)^2+\left(\Delta v_{\mathrm{B}}/2\right)^2},\tag{1}$$

式中：v为入射光频率；v_0为光源频率；v_{B}为布里渊频率偏移；$\Delta v_{\mathrm{B}}=1/\left(\pi\Gamma_{\mathrm{B}}\right)$为增益谱的半峰全宽；$g_0$为自发布里渊增益系数。式(1)右边分母第一项取“+”号表示斯托克斯光，取“−”号表示反斯托克斯光。

2.2 脉冲光布里渊散射谱模型分析

以布里渊斯托克斯光为例，为简化分析，将式(1)写成归一化的形式，即

$$G_{\mathrm{B}}(\omega)=\frac{2\alpha}{\alpha^2+\left(\omega-\omega_{\mathrm{s}}\right)^2},\tag{2}$$

收稿日期：2022-09-01；**修回日期**：2022-10-11；**录用日期**：2022-10-19；**网络首发日期**：2022-11-04

基金项目：国家自然科学基金(52177141)

通信作者：*1073558359@qq.com

式中：α为衰减系数；ω_s为布里渊斯托克斯光的中心角频率。由于功率谱密度与自相关函数是傅里叶变换与傅里叶逆变换的关系，对式(2)进行傅里叶逆变换可得单频连续光在光纤中的布里渊散射光的复数表达式的归一化自相关函数为

$$R_s(t)=\begin{cases}\exp(\alpha t+\mathrm{j}\omega_s t), & -\infty<t<0\\ \exp(-\alpha t+\mathrm{j}\omega_s t), & 0<t<\infty\end{cases}。\tag{3}$$

当光源为脉冲光时，脉冲光在光纤中传播与光纤中的大量声子碰撞产生布里渊散射，此时散射光为大量散射脉冲光的叠加，其自相关函数不再符合式(3)的形式。对于幅度恒定、角频率为ω_0的连续入射光，其光场的复数表达式为$E=E_0\exp(\mathrm{j}\omega_0 t)$，$E_0$为表示入射光幅度常数，因此，功率谱密度函数为冲激函数形式。为方便分析，令光纤入射端的归一化功率谱密度为$\delta(\omega-\omega_0)$，光纤输出端是洛伦兹函数形式的布里渊斯托克斯散射光功率谱密度函数。将光纤布里渊散射过程看作一个系统，该系统的频域模型如图 1 所示。

当工作波长为 1550 nm 波段时，可将图 1 所示光纤布里渊斯托克斯散射系统近似为一个频域线性系统，其等效的频域冲激响应为

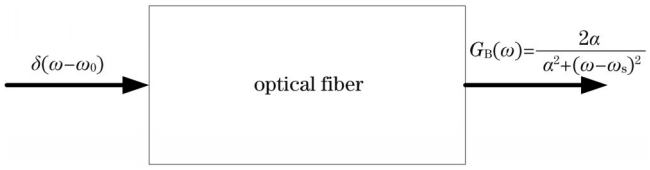

图 1 光纤布里渊斯托克斯散射系统频域模型

Fig. 1 Frequency-domain model of fiber Brillouin Stokes scattering system

$$H_B(\omega)=\frac{2\alpha}{\alpha^2+(\omega-\omega_s+\omega_0)^2}。\tag{4}$$

当入射光是幅度为 1、时间宽度为T的矩形光脉冲时，光场函数为$E=W(t)\exp(\mathrm{j}\omega_0 t)$，其中$W(t)$是幅度为 1、时间宽度为$T$的矩形函数，其自相关函数为

$$R_p(t)=\begin{cases}t/T+1, & -T<t<0\\ -t/T+1, & 0<t<T\\ 0, & \text{others}\end{cases}。\tag{5}$$

式(5)为三角波函数，设其傅里叶变换为$S_W(\omega)$，即矩形函数的功率谱密度为$S_W(\omega)$，将其频移到中心角频率ω_0处，即$S_W(\omega-\omega_0)$为矩形脉冲光的功率谱密度。当图 1 所示的系统输入为$S_W(\omega-\omega_0)$时，系统输出为脉冲光的布里渊散射功率密度谱$G_{sp}(\omega)$，

$$G_{sp}(\omega)=S_W(\omega-\omega_0)\otimes H_B(\omega)=S_W(\omega)\otimes\delta(\omega-\omega_0)\otimes H_B(\omega)=S_W(\omega)\otimes G_B(\omega),\tag{6}$$

式中：$\otimes$表示卷积。直接计算式(6)比较困难。根据频域函数的卷积等于时域函数的乘积，式(6)的傅里叶逆变换(即脉冲光的布里渊斯托克斯散射光的自相关函数)为式(3)与式(5)的乘积，即

$$R_{sp}(t)=\begin{cases}(t/T+1)\exp(\alpha t+\mathrm{j}\omega_s t), & -T<t<0\\ (-t/T+1)\exp(-\alpha t+\mathrm{j}\omega_s t), & 0<t<T\\ 0, & \text{others}\end{cases}。\tag{7}$$

式(7)的傅里叶变换即为脉冲光的布里渊散射功率谱密度：

$$G_{sp}(\omega)=\frac{2\alpha}{\alpha^2+(\omega-\omega_s)^2}+\frac{2\exp(-\alpha T)\left[\alpha^2+(\omega-\omega_s)^2\right]\cos\left[(\omega-\omega_s)T\right]}{T\left[\alpha^2+(\omega-\omega_s)^2\right]^2}-\frac{4\exp(-\alpha T)\alpha(\omega-\omega_s)\sin\left[(\omega-\omega_s)T\right]+2\left[\alpha^2+(\omega-\omega_s)^2\right]}{T\left[\alpha^2+(\omega-\omega_s)^2\right]^2}。\tag{8}$$

式(8)是脉冲光布里渊斯托克斯散射光的归一化功率谱密度函数，等号右边第一项是洛伦兹函数项，第二项和第三项是脉冲光引起的光谱展宽部分。实际应用中往往采用外差方法将布里渊光谱下频移到电域进行处理。由(8)式得到电域布里渊散射功率谱密度为

$$S_{sp}(f)=\frac{2\alpha A}{\alpha^2+4\pi^2(f-f_B)^2}+\frac{2A\exp(-\alpha T)\left[\alpha^2-4\pi^2(f-f_B)^2\right]\cos\left[2\pi(f-f_B)T\right]}{T\left[\alpha^2+4\pi^2(f-f_B)^2\right]^2}-\frac{8A\exp(-\alpha T)\alpha(f-f_B)\sin\left[2\pi(f-f_B)T\right]+2\left[\alpha^2+4\pi^2(f-f_B)^2\right]}{T\left[\alpha^2+4\pi^2(f-f_B)^2\right]^2},\tag{9}$$

式中：A为表示布里渊散射幅度常数；f_B为布里渊频移，在 1550 nm 波段的单模光纤中，$f_B\approx 11$ GHz。

3　实验及实验结果分析

3.1　实验原理与装置

在BOTDR传感系统中，窄线宽连续光被调制成具有一定重复频率的光脉冲序列并被注入到光纤中，光纤产生背向传输的自发布里渊散射光，携带外界环境信息的背向散射光信号经过光电检测器后变为电信号，对电信号进行采集和处理即可得到布里渊传感信息[17]。BOTDR传感系统结构图如图2所示。

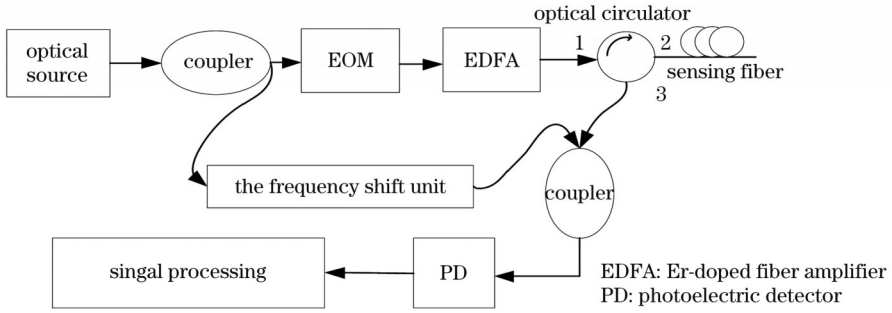

图2　BOTDR系统框图

Fig. 2　Block diagram of Brillouin optical time domain reflectometry (BOTDR) system

光源通过光纤耦合器后分为两路，其中一路用作传感支路，另一路用作本地参考光路。传感光路中的光源信号经过电光调制器(EOM)后被调制成具有一定重复频率的光脉冲，调制后的光脉冲经过光学放大器，然后在光环形器的端口1注入，再输入到与光环形器端口2相连的传感光纤中。后向输出光分为拉曼散射光、布里渊散射光、瑞利散射光和光纤端面反射光等，而后向反射光经由光环行器端口3输出；后向传输的自发布里渊光中包含有传感光纤的温度和应力信息。根据基本结构，BOTDR系统可以分为直接检测系统和外差检测系统[18]。入射光与布里渊散射光之间的频率偏移量相对较小，所以通过直接测量方法无法获取自发布里渊散射光的信息。鉴于此，这里采用了外差检测系统。利用耦合器输出的参考光与布里渊散射光进行差分检测，光信号经过光电检测器后转换成电信号，对该电信号进行采集和处理即可获得传感光纤的温度或应力的沿纤分布信息。

3.2　实验结果与分析

实验中使用的是Advantest公司的N8511型BOTDR设备，采用的脉冲宽度分别为50、20、10 ns。布里渊频域测量从10.72 GHz开始，到11.00 GHz结束，传感光纤长度为3000 m，选取500 m处的布里渊功率谱采样值。入射光的散射谱采样值数目为141个$\left[(f_k, S_k), k=1, 2, 3, \cdots, 141, f_k\right.$和$\left.S_k$表示布里渊散射谱采样点的横纵坐标$\right]$，频率采样间隔为2 MHz，起始频率为10.72 GHz，结束频率为11.00 GHz。

采用式(9)对不同宽度的脉冲光在传感光纤500 m处的布里渊频域采样值进行曲线拟合。为了对比，采用式(9)等号右侧第一项洛伦兹函数对采样数据进行曲线拟合，拟合采用Levenberg-Marquart算法。拟合所得各参数结果以及拟合误差分别如表1和表2所示。

表1　参数拟合结果

Table 1　Results of parameter fitting

Pulse width / ns	A		α		f_B /GHz	
	Lorentz function	Pulsed light function	Lorentz function	Pulsed light function	Lorentz function	Pulsed light function
50	0.0004949	0.0004929	0.1878	0.16490	10.85495	10.85505
20	0.0004549	0.0004409	0.2068	0.13550	10.85561	10.85622
10	0.0004752	0.0004284	0.2568	0.07264	10.85830	10.85875

表2　拟合误差

Table 2　Fitting error

Pulse width /ns	Fitting error	
	Lorentz function	Pulsed light function
50	0.000003447	0.000003130
20	0.000003077	0.000001443
10	0.000004996	0.000001632

由表2和图3～5可以看出，使用本文所得的脉冲光函数对布里渊散射谱数据进行拟合的准确度要优于传统的洛伦兹函数，而且随着入射脉冲光宽度变窄，使用脉冲光函数进行拟合能够更有效地提高布里渊散射谱的拟合精度。

为了更准确地说明实验结果，每50 m传感光纤采集一次布里渊散射谱数据，共采集了1000 m恒温

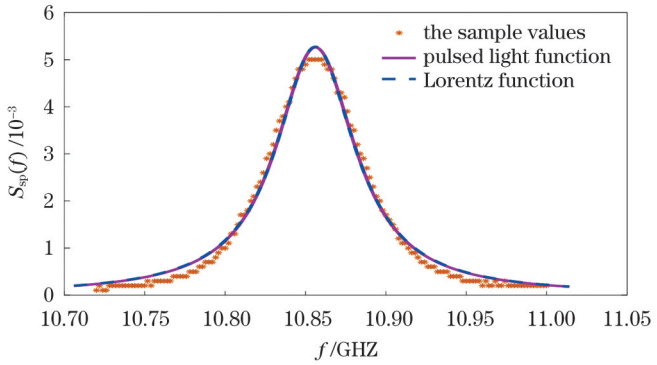

图 3　50 ns脉冲宽度下的曲线拟合对比

Fig. 3　Curve fitting comparison at 50 ns pulse width

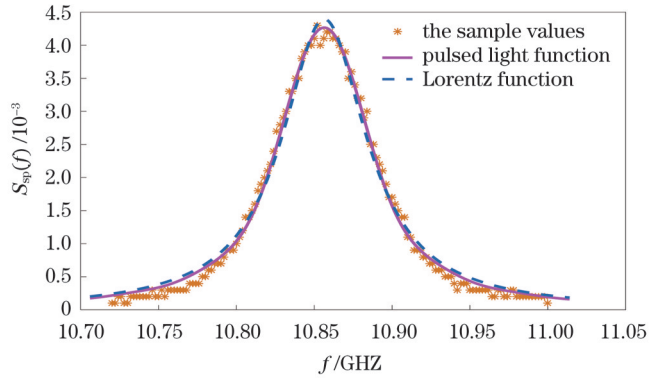

图 4　20 ns脉冲宽度下的曲线拟合对比

Fig. 4　Curve fitting comparison at 20 ns pulse width

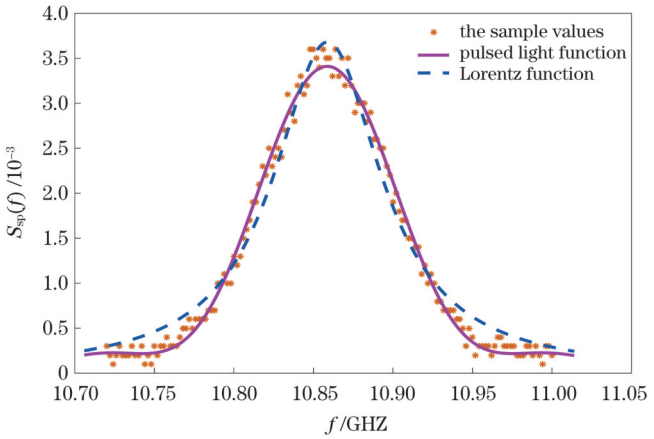

图 5　10 ns脉冲宽度下的曲线拟合对比

Fig. 5　Curve fitting comparison at 10 ns pulse width

零应变传感光纤的布里渊散射谱数据，然后采用式(9)所示函数和洛伦兹函数对这些数据进行拟合。采用差平方和(SSE)、均方根误差(RMSE)、均方差(MSE)、拟合度(R^2)等4个指标对拟合结果进行对比。其中：SSE表示观测值与拟合值差的平方和，该值越小，表明模型选择得越合适，拟合结果越准确；RMSE表示数据的离散程度；MSE表示预测数据与观测数据对应点误差平方和的均值；R^2表示曲线拟合的优劣，其值最大为1，越接近1表明对因变量的解释力越强。入射脉冲光的脉冲宽度分别为50、20、10 ns。图6～8分别给出了50、20、10 ns脉冲宽度下的拟合指标对比图。由图6可以看出，在50 ns脉冲宽度下，脉冲光函数与洛伦兹函数拟合结果的SSE、RMSE、MSE、R^2指标性能相近，使用洛伦兹函数进行拟合的平均拟合度为0.99077，使用本文推导的脉冲光函数拟合的平均拟合度为0.991656。随着传感距离增加，拟合度可能会出现下降。这是因为随着距离增加，布里渊散射信号受到噪声的干扰也会增大。如图7所示，当脉冲宽度为20 ns时，脉冲光函数拟合结果的SSE、RMSE、MSE、R^2指标都优于洛伦兹函数拟合结果的相应指标，使用洛伦兹函数进行拟合的平均拟合度为0.98805，而使用本文推导的脉冲光函数拟合的平均拟合度可以达到0.994345。如图8所示，当脉冲宽度为10 ns时，脉冲光函数拟合结果的SSE、RMSE、MSE、R^2指标都显著优于传统洛伦兹函数拟合结果的相应指标，用洛伦兹函数进行拟合的平均拟合度仅为0.97249，而使用本文推导的脉冲光函数进行拟合的平均拟合度可以达到0.990030。

综上可以得出，随着布里渊传感系统入射脉冲光的脉冲宽度变窄，进行脉冲光自发布里渊散射谱拟合时，利用式(9)所示的脉冲光布里渊散射功率谱密度函数进行拟合的效果要优于洛伦兹函数的拟合效果。

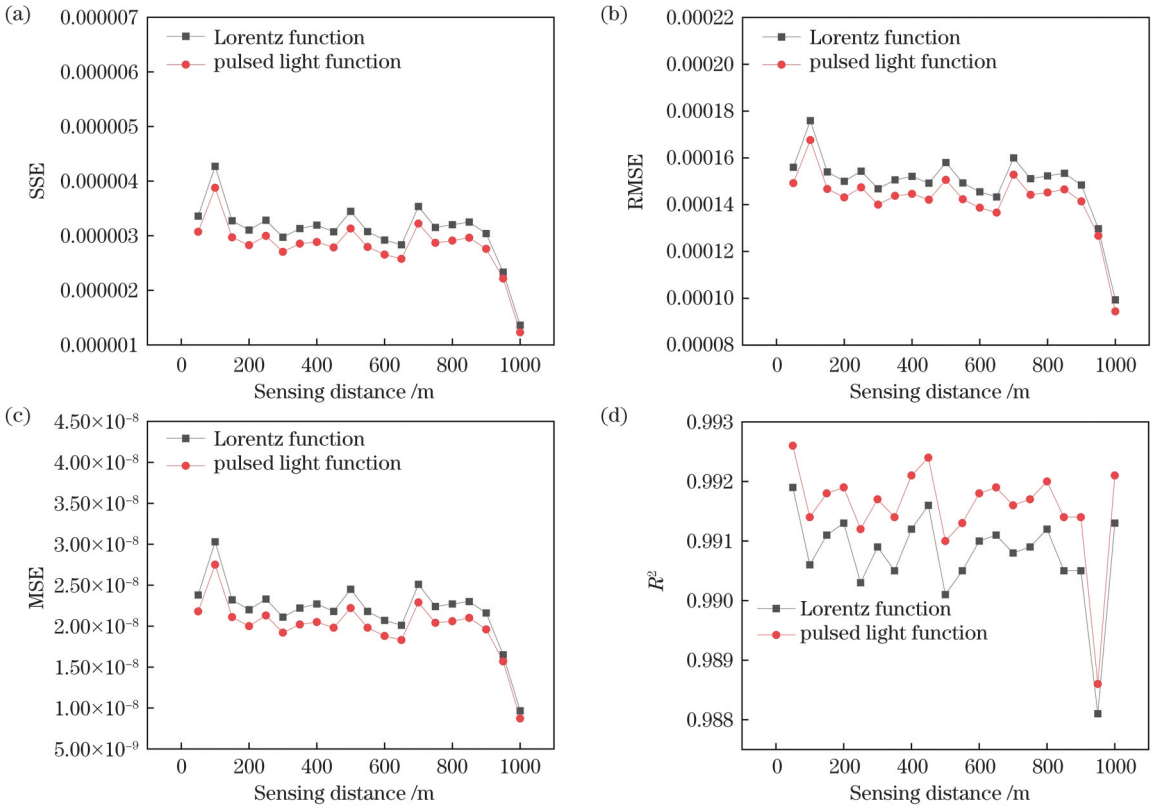

图 6　50 ns 脉冲宽度下的拟合指标对比。(a)SSE;(b)RMSE;(c)MSE;(d)R^2

Fig. 6　Comparison of fitting indexes at 50 ns pulse width. (a) SSE; (b) RMSE; (c) MSE; (d) R^2

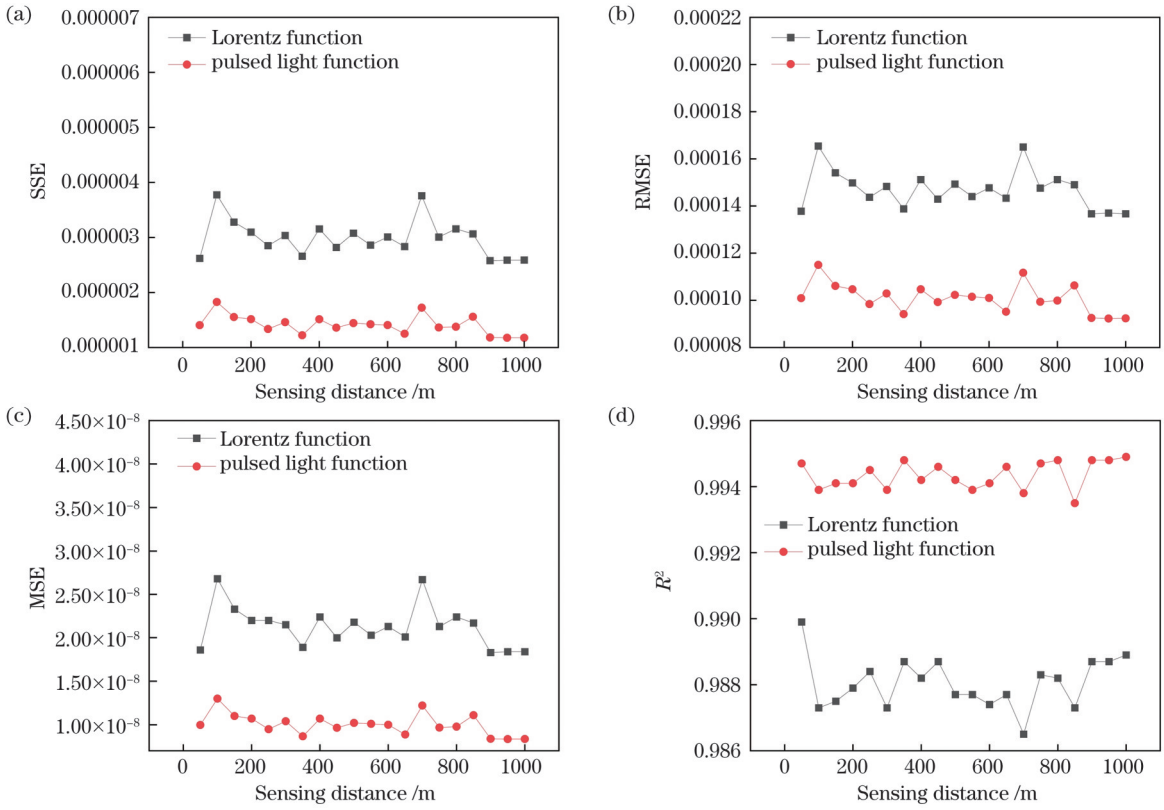

图 7　20 ns 脉冲宽度下的拟合指标对比。(a)SSE;(b)RMSE;(c)MSE;(d)R^2

Fig. 7　Comparison of fitting indexes at 20 ns pulse width. (a) SSE; (b) RMSE; (c) MSE; (d) R^2

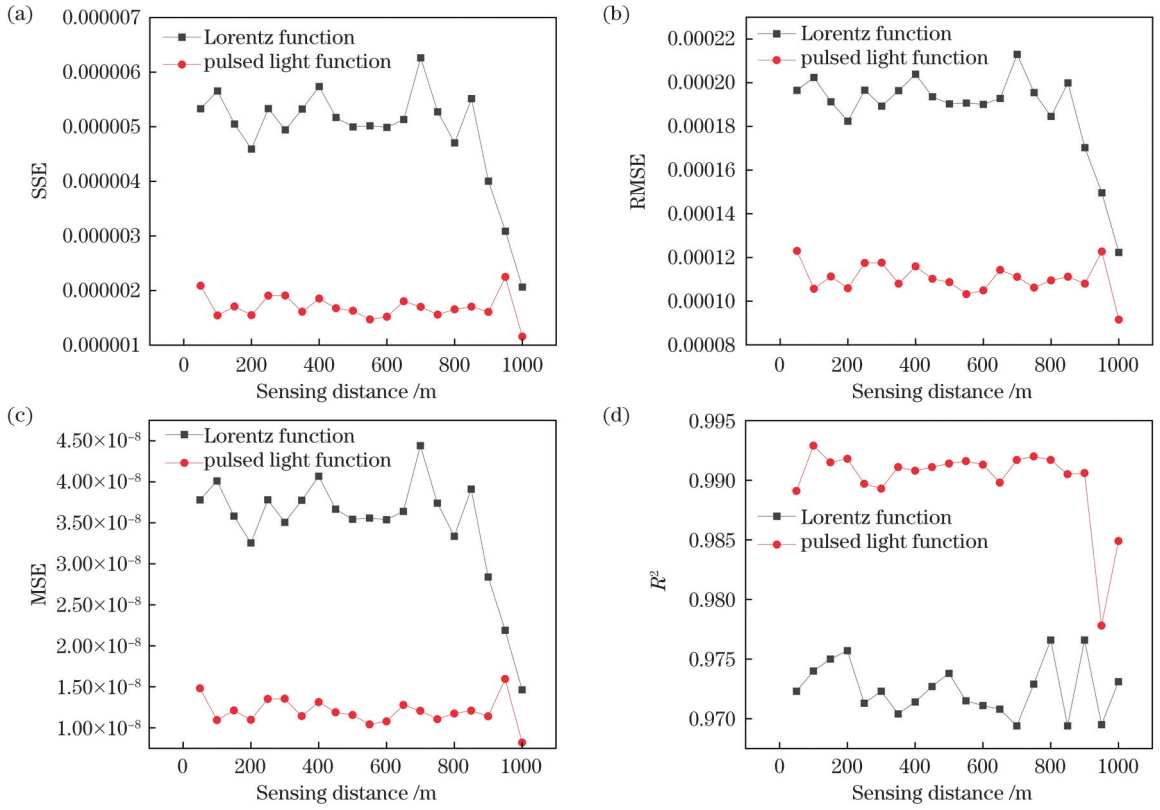

图 8　10 ns 脉冲宽度下的拟合指标对比。(a) SSE; (b) RMSE; (c) MSE; (d) R^2

Fig. 8　Comparison of fitting indexes at 10 ns pulse width. (a) SSE; (b) RMSE; (c) MSE; (d) R^2

4　结　　论

针对脉冲光布里渊散射谱在用洛伦兹函数进行拟合时存在拟合误差较大的问题，笔者分析并推导了脉冲光布里渊散射功率谱密度函数，并采用布里渊光时域反射仪系统进行了实验验证。结果表明：随着入射脉冲光的脉冲宽度变窄，采用所提函数进行脉冲光布里渊散射谱拟合时，拟合结果的 SSE、RMSE、MSE、R^2 指标均优于洛伦兹函数拟合结果的对应指标。所提拟合方法的拟合准确度更高，参数估计更准确。

参　考　文　献

[1] 韩国庆，刘显明，雷小华，等. 光纤传感技术在航空发动机温度测试中的应用[J]. 仪器仪表学报，2022，43(1): 145-164.
Han G Q, Liu X M, Lei X H, et al. Application of optical fiber sensing in aero-engine temperature test[J]. Chinese Journal of Scientific Instrument, 2022, 43(1): 145-164.

[2] Nan Y G, Xie W P, Min L, et al. Real-time monitoring of wind-induced vibration of high-voltage transmission tower using an optical fiber sensing system[J]. IEEE Transactions on Instrumentation and Measurement, 2020, 69(1): 268-274.

[3] Khan F, Donder A, Galvan S, et al. Pose measurement of flexible medical instruments using fiber Bragg gratings in multi-core fiber [J]. IEEE Sensors Journal, 2020, 20(18): 10955-10962.

[4] 李振，王纪强，赵林，等. 基于差压原理的矿用光纤光栅风速传感器[J]. 红外与激光工程，2018，47(4): 0422002.
Li Z, Wang J Q, Zhao L, et al. Mine wind speed sensor using fiber Bragg grating based on differential pressure principle[J]. Infrared and Laser Engineering, 2018, 47(4): 0422002.

[5] Fan H J, Li Y Q, Zhang L X, et al. Multimode fiber temperature sensing based on BOTDR[J]. Laser Journal, 2022, 43(1): 74-80.

[6] 王晨，席丽霞，张阳安，等. 提升小波阈值联合累加平均的 BOTDR 系统降噪方案[J]. 中国激光，2021，48(17): 1706001.
Wang C, Xi L X, Zhang Y A, et al. Denoising scheme of BOTDR system using the combination of lifting wavelet threshold and cumulative average[J]. Chinese Journal of Lasers, 2021, 48 (17): 1706001.

[7] 张洪英，杨志远，崔荣鹏，等. 基于 BOTDR 的海上风力发电机桩基水平荷载性能研究[J]. 光学学报，2021，41(13): 1306016.
Zhang H Y, Yang Z Y, Cui R P, et al. Horizontal load test on offshore wind turbine pile foundation based on BOTDR[J]. Acta Optica Sinica, 2021, 41(13): 1306016.

[8] 梁浩，张旭苹，李新华，等. 布里渊背向散射光谱数据拟合算法设计与实现[J]. 光子学报，2009，38(4): 875-879.
Liang H, Zhang X P, Li X H, et al. Design and implementation of data fitting algorithm for Brillouin back scattered-light spectrum data[J]. Acta Photonica Sinica, 2009, 38(4): 875-879.

[9] 何玉钧，尹成群，李永倩，等. 一个新型的基于全光纤 Mach-Zehnder 干涉仪 BOTDR 系统[J]. 光子学报，2004，33(6): 721-724.
He Y J, Yin C Q, Li Y Q, et al. A novel BOTDR system based on all fiber Mach-Zehnder interferometer[J]. Acta Photonica Sinica, 2004, 33(6): 721-724.

[10] Zhang Y Z, Xu Z Y, Wang R, et al. Simultaneous strain and temperature measurement using a Brillouin scattering based superstructure fiber grating filter[C]//2007 8th International Conference on Electronic Measurement and Instruments, August 16-18, 2007, Xi'an, China. New York: IEEE Press, 2007: 607-611.

[11] Wang S, Luan L J. The applied research of BOTDR technology in underground engineering[C]//2011 Symposium on Photonics and Optoelectronics (SOPO), May 16-18, 2011, Wuhan, China. New York: IEEE Press, 2011.

[12] Xiao S H, Li L. New fitting method for Brillouin-based scattering spectrum of fibre-optic distributed sensing systems[J]. Optical Technique, 2009, 35(6): 897-900, 904.

[13] 张燕君, 张书国, 付广伟, 等. 布里渊散射谱参数提取问题的混合优化算法研究与应用[J]. 光谱学与光谱分析, 2012, 32(4): 915-920.
Zhang Y J, Zhang S G, Fu G W, et al. Research on and application of hybrid optimization algorithm in Brillouin scattering spectrum parameter extraction problem[J]. Spectroscopy and Spectral Analysis, 2012, 32(4): 915-920.

[14] Chen X J, Yu H Y, Huang W Z. A high accurate fitting algorithm for Brillouin scattering spectrum of distributed sensing systems based on LSSVM networks[C]//2021 International Conference on Electronic Information Engineering and Computer Science (EIECS), September 23-26, 2021, Changchun, China. New York: IEEE Press, 2021: 107-110.

[15] Wang F, Zhan W W, Lu Y G, et al. Determining the change of Brillouin frequency shift by using the similarity matching method [J]. Journal of Lightwave Technology, 2015, 33(19): 4101-4108.

[16] 尚秋峰, 胡雨婷, 刘薇. BOTDA传感系统的布里渊频移提取方法研究进展[J]. 半导体光电, 2017, 38(5): 633-638, 669.
Shang Q F, Hu Y T, Liu W. Research on Brillouin frequency shift extraction method of BOTDA sensing system[J]. Semiconductor Optoelectronics, 2017, 38(5): 633-638, 669.

[17] 王健健. BOTDR传感系统性能优化方法研究[D]. 北京: 华北电力大学, 2021.
Wang J J. Research on performance optimization methods of BOTDR sensing system[D]. Beijing: North China Electric Power University, 2021.

[18] 包宇奔, 孙军强, 黄强. 布里渊光时域反射仪分布式光纤传感研究进展[J]. 激光与光电子学进展, 2020, 57(21): 210002.
Bao Y B, Sun J Q, Huang Q. Distributed fiber sensor based on Brillouin optical time domain reflection technique[J]. Laser & Optoelectronics Progress, 2020, 57(21): 210002.

Optical Fiber Brillouin Scattering Spectrum Fitting of Pulsed Light

Yang Zhi[1,2], Wang Zhen[1*], Li Yongqian[1,2], Lü Anqiang[1,2]

[1]*Department of Electronic and Communication Engineering, North China Electric Power University, Baoding* 071003, *Hebei, China*;

[2]*Hebei Key Laboratory of Power Internet of Things Technology, North China Electric Power University, Baoding* 071003, *Hebei, China*

Abstract

Objective Optical fiber sensing is an essential aspect of sensing technology. An optical fiber can be used as a medium through corresponding technical approaches to detect changes in the wavelength and frequency of optical signals, indirectly monitoring changes in the external environment. Because of its significant anti-electromagnetic interference ability, optical fiber sensing technology can work satisfactorily in strong magnetic environments, and it exhibits high-temperature resistance and good corrosion resistance in diverse areas such as aerospace, medical testing, civil engineering, power monitoring, and military applications. This method has received increasing attention and applications. Distributed fiber-optic sensing utilizes the nonlinear scattering properties of light as it travels through the fiber to monitor changes in the external environment, such as the temperature and pressure along the fiber. The Brillouin optical time-domain reflectometer can detect changes in the external environment by measuring the shift in the center frequency of the spontaneous Brillouin scattering spectrum of the pulsed light in the fiber. Brillouin-distributed fiber-optic sensing enables long-distance temperature and stress measurements. This technology has higher measurement accuracy and spatial resolution, and it can be applied to longer measurement distances than other sensing technologies. This technology plays a critical role in various industrial applications. Currently, extraction of the center frequency of the Brillouin scattering spectrum is typically performed according to the Lorentzian function. The frequency-sampled values of the Brillouin scattering spectra were measured using equally spaced frequency sweeps and fitted using a Lorentzian function. The frequency value corresponding to the center point of the Lorentz curve obtained by fitting is the center frequency of the Brillouin scattering spectrum, and the Brillouin frequency shift is obtained by subtracting the value from the frequency of the light source. The Brillouin scattering spectrum of single-frequency continuous light satisfies the Lorentz function distribution, but the Brillouin scattering spectrum of pulsed light does not satisfy the Lorentz function distribution. In other words, the spectrum of the incident signal is broadened when pulse modulation is performed, and the Brillouin scattering spectrum is also broadened. Hence, more accurate model fitting results cannot be obtained by fitting a general Lorentzian parameter model. In this study, the expression of the optical fiber Brillouin scattering spectrum function of the pulsed light signal, which significantly improves the fitting accuracy of the Brillouin scattering spectrum, was derived.

Methods In this study, a significant fitting error was observed when the pulsed light Brillouin scattering spectrum was fitted using the traditional Lorentzian curve. Stokes light and anti-Stokes light were used as examples, and the functional expression of the fiber Brillouin scattering spectrum of pulsed light was derived via theoretical analysis. The fitting accuracy was improved using this functional expression. A Brillouin optical time-domain reflectometer was used for measurements. When the light source signal flows through the optical coupler, it is divided into two paths: one is used as the sensing branch, and the other is used as the local reference optical path. The optical signal of the sensing branch was modulated into an optical pulse with a specific repetition frequency after passing through the modulator. The optical signal reflected by the sensing branch after passing through the sensing optical fiber was differentially detected with the local reference optical path, and the signal was collected. The Lorentz fitting and pulsed light function derived in this study were used to fit the measurement results, and the fitting accuracy values were compared.

Results and Discussions First, the sampling value of the Brillouin power spectrum of 500 m sensing fiber was selected. The fitting results show a significant error in the fitting of the Lorentz function, which can be significantly reduced using the pulsed light function (Fig. 3). The Brillouin scattering spectrum data were collected every 50 m of the sensing fiber to make the experimental results universal, and the scattering data of the 1000 m constant-temperature zero-strain sensing fiber were collected. The Lorentzian function and pulsed light function derived in this study were used to fit. The functions were compared based on four aspects: the sum of squares of differences, root-mean-square error, mean square error, and goodness of fit (Figs. 4–7). The experimental results show that using the pulsed light function for fitting, the difference sum of squares, root-mean-square error, and mean square error are significantly smaller than those of the Lorentzian function fitting, and the degree of fitting of the pulsed light function is significantly higher than that of the Lorentzian function. Therefore, the fitting performance of the pulse light scattering power spectral density function is higher than that of the Lorentzian function.

Conclusions The fitting error of the Brillouin scattering spectrum using the Lorentz function is significant, and the central frequency cannot be extracted with high precision, which leads to inaccurate monitoring of external environmental changes. Through theoretical research, the Brillouin scattering power spectral density function of pulsed light was obtained, which improved the fitting accuracy. Through the Brillouin optical time-domain reflectometer sensing experiment, the measured Brillouin scattering spectrum data were fitted using different methods, and the fitting was obtained using the pulsed-light Brillouin scattering power spectral density function. The higher the fitting accuracy, the more accurate would be the parameter estimation and the smaller would be the error. This study can provide valuable information for applying and developing distributed optical fiber sensing.

Key words fiber optics; Brillouin scattering; Brillouin frequency shift; Lorentz function; data fitting